Chaos and Instability in a Power System: Subharmonic-Resonant Case

M. A. NAYFEH*, A. M. A. HAMDAN**, and A. H. NAYFEH*

*Virginia Polytechnic Institute and State University, Blacksburg, VA 24061, U.S.A.

**Bahrain University, Isa Town, Bahrain.

Abstract. The response of a single-machine quasi-infinite busbar system to the simultaneous occurrence of principal parametric resonance and subharmonic resonance of order one-half is investigated. By numerical simulations we show the existence of oscillatory solutions (limit cycles), period-doubling bifurcations, chaos, and unbounded motions (loss of synchronism). The method of multiple scales is used to derive a second-order analytical solution that predicts (a) the onset of period-doubling bifurcations, which is a precursor to chaos and unbounded motions (loss of synchronism), and (b) saddle-node bifurcations, which may be precursors to loss of synchronism.

Key words: Power systems, loss of synchronism, chaos, bifurcations.

1. Introduction

In power-system dynamics it is often desirable to concentrate on a single machine. For convenience, the rest of the system is considered to be an infinite busbar whose voltage and frequency are constant. An interesting and more realistic concept is that of a quasi-infinite busbar introduced by Tamura *et al.* [1]. In a quasi-inifinite busbar the voltage and phase of the busbar are time-varying. Tamura *et al.* formulated the single-machine quasi-infinite busbar system (SMQIBS) as a Mathieu equation. In an earlier paper, Hamdan and Nayfeh [2] reformulated the problem and included quadratic and cubic nonlinearities. The method of multiple scales [3, 4] was used to obtain a first-order closed-form approximate solution of the resulting nonlinear differential equation. They studied the simultaneous effect of a principal parametric resonance and a subharmonic resonance of order one-half. In such a case, the frequency Ω of the periodic variations in the magnitude and the phase of the quasi-infinite busbar is nearly equal to twice the linear undampled natural frequency ω_0 of the system (i.e., $\Omega \approx 2\omega_0$). They showed the coexistence of stable and unstable oscillatory solutions and the existence of a subcritical instability. They found that the solution exhibits pitchfork and cyclic-fold bifurcations.

In this paper, we use numerical simulations and perturbation analyses to investigate the behavior of the system near the simultaneous occurrence of a principal parametric resonance and a subharmonic resonance of order one-half. Numerical simulations are used to show that the combined effect of these resonances leads to complicated dynamics. As the excitation frequency is varied, we demonstrate that the response undergoes a sequence of period-doubling bifurcations culminating in chaos, after which the solution becomes unbounded. The effect of varying the voltage and frequency of the quasi-infinite busbar is studied by forming a bifurcation diagram in a two parameter space, indicating where saddle-node instabilities, period-doubling bifurcations, and loss of synchronism occur. The effect of a variation in either the voltage or the phase of the quasi-infinite busbar on the basins of attraction is also studied. Similar studies were conducted by Grebogi, Ott, and Yorke [5], Nayfeh and Sanchez [6], and Soliman and Thompson [7] for other

Nonlinear Dynamics **2**: 53–72, 1991.

systems. Using numerical simulations alone to locate the regions of complex behavior requires a lot of time and effort. So it is of interest to develop approximate solutions that will reduce the computational time and effort. First, we investigated the use of the first-order perturbation solution of Hamdan and Nayfeh [2]. We found that this expansion predicts fairly accurately the period-one motions and their bifurcations into period-two motions for small excitation amplitudes. However, as the excitation amplitude increases, we found that the first-order perturbation solution becomes less accurate. Therefore, we use the method of multiple scales to determine a second-order approximate solution that improves on the accuracy of the solution given by Hamdan and Nayfeh [2], and whose loss of stability agrees fairly well with the onset of period-doubling bifurcations, which is a precursor to chaos and loss of synchronism.

2. Formulation

The equation of motion for the rotor of the machine shown in Figure 1 can be written as [8]

$$\frac{2H}{\omega_R}\frac{\mathrm{d}^2\theta}{\mathrm{d}t^2} + D\frac{\mathrm{d}\theta}{\mathrm{d}t} = P_m - \frac{V_G V_B}{X_G}\sin(\theta - \theta_B)\,, \tag{1}$$

where

$$V_B = V_{B0} + V_{B1}\cos(\Omega t + \phi_v)\,, \tag{2}$$

$$\theta_B = \theta_{B0} + \theta_{B1}\cos(\Omega t + \phi_\theta)\,. \tag{3}$$

Here, θ is the rotor angle measured with respect to a synchronously rotating reference frame moving with the constant angular velocity ω_R, H is the inertia constant of the machine, D is the damping coefficient, and P_m is the mechanical power input to the machine. The sinusoidal term in equation (1) corresponds to the electrical power output of the machine, V_G is the voltage of the machine, X_G is the transient reactance of the machine, V_B is the voltage of the busbar, and θ_B is the phase of the busbar. The parameters H, ω_R, D, P_m, V_G, X_G, V_{B0}, V_{B1}, θ_{B0}, θ_{B1}, Ω, φ_v, ϕ_θ are assumed to be constant. Equation (1) is often called the swing equation. For an infinite busbar, $V_{B1} = 0$ and $\theta_{B1} = 0$, whereas for a quasi-infinite busbar [1], either V_{B1} or θ_{B1} or both are different from zero.

To carry out a perturbation analysis, we find it convenient to apply the following transformation:

$$\theta - \theta_B = \delta_0 + \eta\,, \tag{4}$$

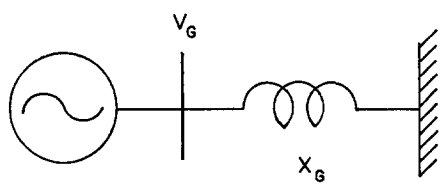

Fig. 1. Single-machine quasi-infinite busbar system.

where θ_0 is the operating value of θ around which the variation $\Delta\theta = \theta - \theta_0$ takes place. Thus, it can be obtained from equation (1) by setting $V_{B1} = \theta_{B1} = 0$ and $d\theta/dt = d^2\theta/dt^2$. The result is

$$\sin(\theta_0 - \theta_{B0}) = \sin \delta_0 = \frac{X_G P_m}{V_G V_{B0}} . \tag{5}$$

Thus, it follows from equations (3) and (4) that

$$\eta = \Delta\theta - \theta_{B1} \cos(\Omega t + \phi_\theta) . \tag{6}$$

Substituting equations (4) and (5) into equation (1), expanding $\sin(\delta_0 + \eta)$ in a Taylor series around $\delta = \delta_0$, and retaining terms up to third order, we obtain the following modified swing equation:

$$\begin{aligned} &\frac{d^2\eta}{dt^2} + \frac{\omega_R D}{2H} \frac{d\eta}{dt} + K\eta = \alpha_2 \eta^2 + \alpha_3 \eta^3 \\ &+ F_1 \eta \cos(\Omega t + \phi_v) + F_2 \eta^2 \cos(\Omega t + \phi_v) + F_3 \eta^3 \cos(\Omega t + \phi_v) \\ &+ G_1 \cos(\Omega t + \phi_\theta) + G_2 \sin(\Omega t + \phi_\theta) + G_3 \cos(\Omega t + \phi_v) , \end{aligned} \tag{7}$$

where

$$K = \frac{V_G V_{B0} \omega_R \cos \delta_0}{2HX_G} , \quad \alpha_2 = \frac{1}{2} K \tan \delta_0 , \quad \alpha_3 = \frac{1}{6} K , \tag{8}$$

$$F_1 = -\frac{V_{B1}}{V_{B0}} K , \quad F_2 = \frac{V_{B1}}{2V_{B0}} K \tan \delta_0 , \quad F_3 = \frac{V_{B1}}{6V_{B0}} K , \tag{9}$$

$$G_1 = \Omega^2 \theta_{B1} , \quad G_2 = \frac{\Omega D \omega_R \theta_{B1}}{2H} , \quad G_3 = -\frac{V_{B1}}{V_{B0}} K \tan \delta_0 . \tag{10}$$

It is clear from equations (7) and (8) that the linear undamped natural frequency ω_0 of the machine is given by $\sqrt{K}$ and that it is zero when $\cos \delta_0 = 0$. The latter case is excluded in the following analysis. The influence of the quasi-infinite busbar appears as parametric excitations (time-varying coefficients) and external excitations (inhomogeneous terms). The external excitations in equation (7) can be combined into a single external-excitation term as follows:

$$G \cos(\Omega t + \phi_e) = G_1 \cos(\Omega t + \phi_\theta) + G_2 \sin(\Omega t + \phi_\theta) + G_3 \cos(\Omega t + \phi_v) . \tag{11}$$

A resonance occurs when a small excitation leads to a large response in η. The strongest parametric resonance takes place when $\Omega \approx 2\omega_0$, which is called principal parametric resonance. The strongest external resonance occurs when $\Omega \approx \omega_0$, which is called primary resonance. Another external resonance occurs when $\Omega \approx 2\omega_0$, which is called subharmonic resonance of order one-half. In this paper, we consider the simultaneous effect of a principal parametric resonance and a subharmonic resonance of order one-half.

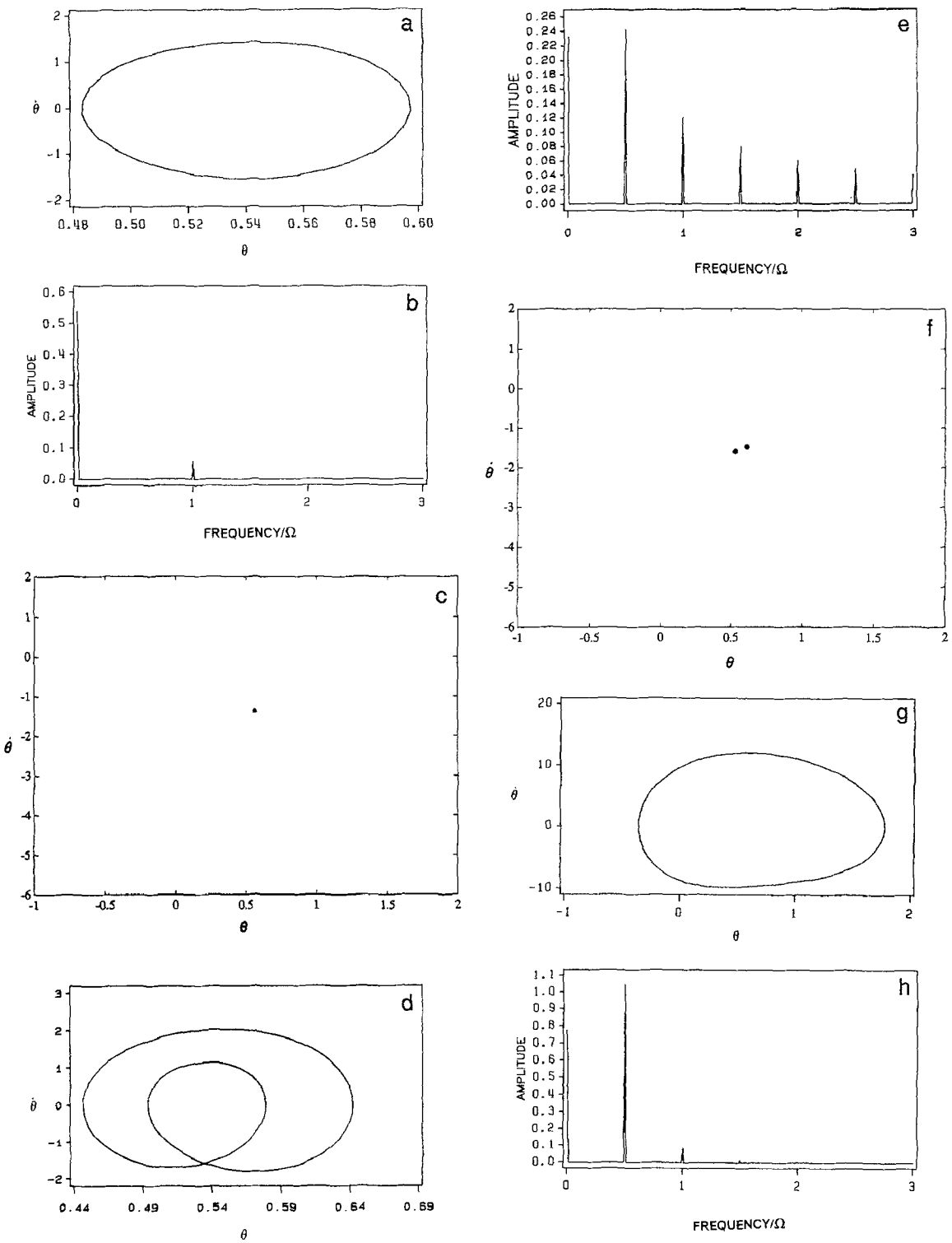

Fig. 2. Numerical simulation: (a)–(c) period-one attractor at $\Omega = 26.0$ rad/sec; (d)–(f) period-two attractor at $\Omega = 24.155$ rad/sec; (g)–(i) period-two attractor at $\Omega = 21.03$ rad/sec; (j)–(l) period-four attractor at $\Omega = 19.416$ rad/sec; (m)–(o) chaos at $\Omega = 19.374$ rad/sec; (p) loss of synchronism at $\Omega = 19.373$ rad/sec. For each attractor, the first figure shows the phase plane, the second figure shows the FFT, and the third figure shows the Poincaré section.

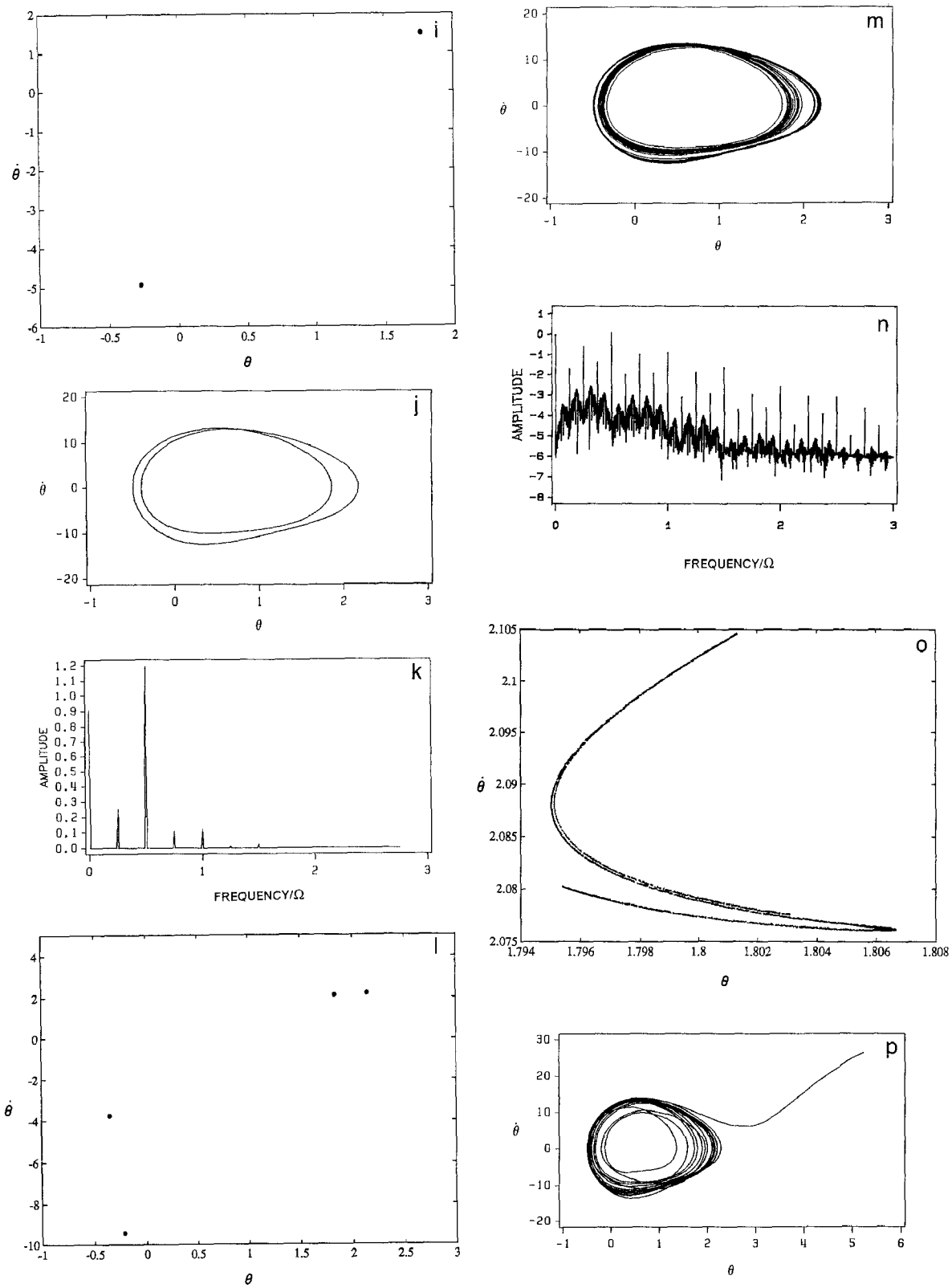

Fig. 2 (continued).

3. Numerical Simulation

Equations (1)–(3) were simulated on the digital computer by using fifth- and sixth-order Runge–Kutta algorithms. The parameters of the system are listed in Appendix A. We studied the effect of varying the frequency Ω of the voltage and phase variations of the quasi-infinite busbar near the subharmonic resonance of order one-half; that is, $\Omega \approx 2\omega_0 = 23.2294$ rad/sec. In what follows, we refer to this frequency Ω as the excitation frequency. The effect of varying the excitation frequency Ω is shown in Figure 2 when $V_{B1} = 0.2$ per unit, $\theta_{B1} = 0.2$ rad, $\theta_{B0} = 0$, $V_{B0} = 1$ per unit, $D = 0.008$ units, $\omega_R = 120\pi$ rad./sec., $H = 2.37S$, $X_G = 0.645$ per unit, and $P_m = 1$ per unit.

For Ω larger than $2\omega_0$, the steady-state solution (attractor) is periodic having the period $2\pi/\Omega$. The phase portrait corresponds to a period-one limit cycle (Figure 2a). This can be verified by observing the corresponding power spectrum obtained by using a fast Fourier transform FFT (Figure 2b) and Poincaré section (Figure 2c) obtained by sampling the data every $T = 2\pi/\Omega$ sec; the FFT consists of frequency components at Ω and its harmonics and the Poincaré section contains only one point. As Ω is decreased, the period-one orbit deforms until Ω reaches the threshold value 24.155 rad/sec, where the period-one attractor loses stability and gives way to a period-two attractor (Figure 2d) with the period $4\pi/\Omega$. The FFT (Figure 2e) and Poincaré section (Figure 2f) verify the occurrence of a period-doubling bifurcation. The FFT has new frequency components at $\Omega/2$, $3\Omega/2$, $5\Omega/2$, ... and their harmonics and the Poincaré section contains two points. As Ω is decreased further the amplitude of the subharmonic component increases compared with the amplitude of the main harmonic, resulting in a period-two attractor with only one loop (Figure 2g). This can be clearly seen in the FFT (Figure 2h), the amplitude of the component at Ω is much smaller than the amplitude of the component at $\Omega/2$. In Figure 2d, the response consists of two fundamental frequencies Ω and $\Omega/2$ and hence the phase plane has a "figure eight" shape. However, due to the fact that the amplitude of the subharmonic is very large compared with the amplitude of the fundamental harmonic, the response consists of essentially one frequency and hence its phase plane consists of only one loop, as evident in Figure 2g. The Poincaré section has two points (Figure 2i). As Ω is decreased further the period-two attractor goes through a period-doubling bifurcation at $\Omega = 19.65$ rad/sec. The phase portrait shows an attractor consisting of two loops as shown in Figure 2j; the FFT (Figure 2k) shows additional peaks at $\Omega/4$, $3\Omega/4$, and their harmonics and the Poincaré section (Figure 2l) shows four points, the period of this attractor is $8\pi/\Omega$. These period-doubling bifurcations continue as Ω is decreased further and eventually the solution becomes chaotic at $\Omega = 19.374$ rad/sec (Figure 2m). The FFT of the chaotic attractor (Figure 2n) has a broadband power spectrum and the Poincaré section (Figure 2o) shows a strange attractor. The corresponding Liapunov exponents are 0.138, 0.0, -0.771 and the Liapunov dimension is $D_l = 2.18$. We note that the sum of the Liapunov exponents is -0.633, which is approximately equal to $-2\mu = -0.636$, as it should. As Ω is decreased even further ($\Omega = 19.373$ rad/sec), the sequence of bifurcations culminates in an unbounded motion (Figure 2p) (i.e., loss of synchronism).

To investigate the influence of varying the parameters on the system's response, we studied local bifurcations of the solutions of equations (1)–(3) in the two parameter space corresponding to the frequency Ω and amplitude V_{B1} of the voltage of the quasi-infinite busbar (Figure 3). The region on the left side of the bifurcation diagram corresponds to the combined primary and fundamental parametric resonant response. Below the curve S_1, a small limit-cycle attractor having the period $T = 2\pi/\Omega$ exists; below the curve P_1, a large limit-cycle attractor having the

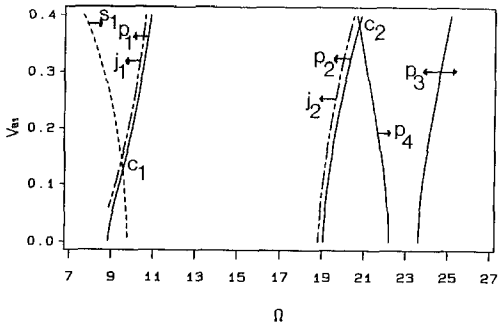

Fig. 3. Bifurcation diagram.

period T exists; below both curves S_1 and P_1, both small and large limit-cycle attractors coexist; and above curves S_1 and J_1, the response of the system is unbounded, which corresponds to loss of synchronism of the machine. If a parameter is varied across S_1 in the direction of the arrow, the small attractor loses stability through a saddle-node bifurcation. The system response will either go unbounded for values of $V_{B1} > C_1$ (i.e., the intersection of curves J_1 and S_1) or jump to the large attractor for values of $V_{B1} < C_1$. The large attractor will go through a sequence of period-doubling bifurcations, culminating in a chaotic attractor, if any of the parameters is varied across P_1 in the direction of the arrow. If a parameter is varied across J_1, the chaotic attractor either goes unbounded if $V_{B1} > C_1$ or jumps to the small attractor if $V_{B1} < C_1$.

The region on the right corresponds to the simultaneous effect of principal parametric resonances and subharmonic resonances of order one-half. For brevity, we will refer to the resulting response as the subharmonic response. Subharmonic responses corresponding to limit-cycle attractors having the period $2T$ exist between the curves P_2 and P_3. To the right of curve P_3 and to the left of curve P_4, limit-cycle attractors having the period T exist. These period-one attractors are essentially the particular solutions of the linearized probem. In the region below both curves P_2 and P_4, both period-one and period-two attractors coexist. Above both curves J_2 and P_4, the response of the system is unbounded.

If P_4 is crossed from left to right the period-one attractor loses stability and jumps to the subharmonic response, yielding a period-two attractor. Also when P_3 is crossed from right to left, the period-one attractor loses stability and jumps to the subharmonic response, yielding a period-two attractor. If P_3 is crossed from left to right, the subharmonic response loses stability and jumps to the period-one attractor. The subharmonic response goes through a sequence of period-doubling bifurcations leading to chaos when P_2 is crossed from right to left. If J_2 is crossed from right to left, the chaotic attractor loses stability; it jumps to the period-one attractor for values of $V_{B1} < C_2$, where C_2 is the intersection of curves J_2 and P_4, and goes unbounded for values of $V_{B1} > C_2$.

Of major importance is the dependence of bounded and unbounded motions on the initial conditions. Hence, we studied the basins of attraction of bounded and unbounded motions for different values of V_{B1} and θ_{B1}. We investigated the region $-1 \leq \theta \leq 3.5$ and $-25 \leq \dot{\theta} \leq 15$ with a grid of 400×450 initial conditions. For each set of initial conditions, we integrated equations (1)–(3) by using fifth- and sixth-order Runge–Kutta algorithms for at least 20 cycles, sometimes 100 or 400 cycles. If the solution became unbounded, we marked the corresponding point by a black dot; otherwise, we marked it by a white dot. By changing one of the system parameters, we observed the metamorphoses that the basins of attraction undergo. Figure 4 shows a series of

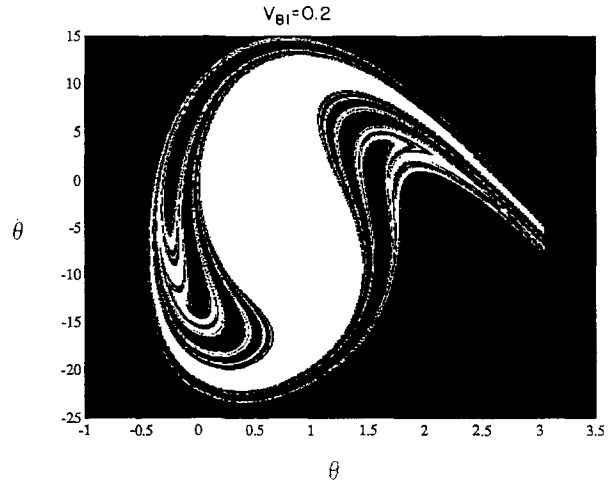

a

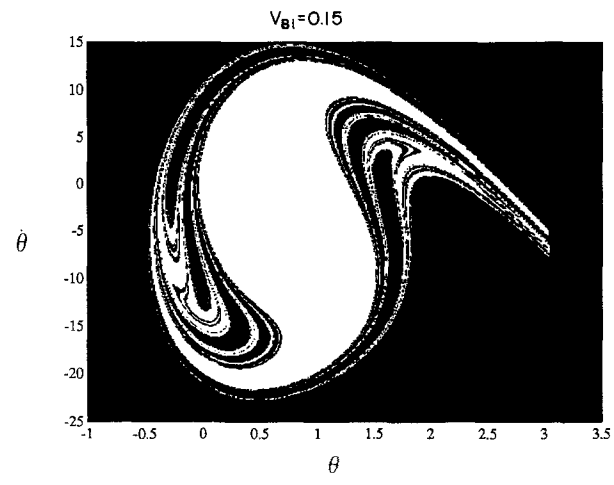

b

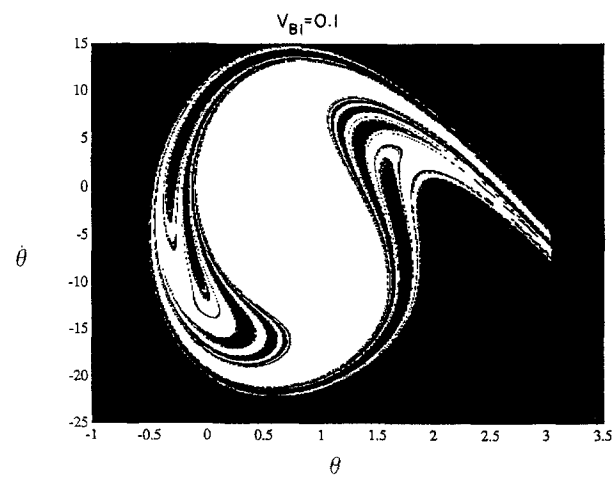

c

Fig. 4. Basins of attraction (θ vs. θ) for $\Omega = 19.375$ rad/sec and $\theta_{B1} = 0.2$ radians

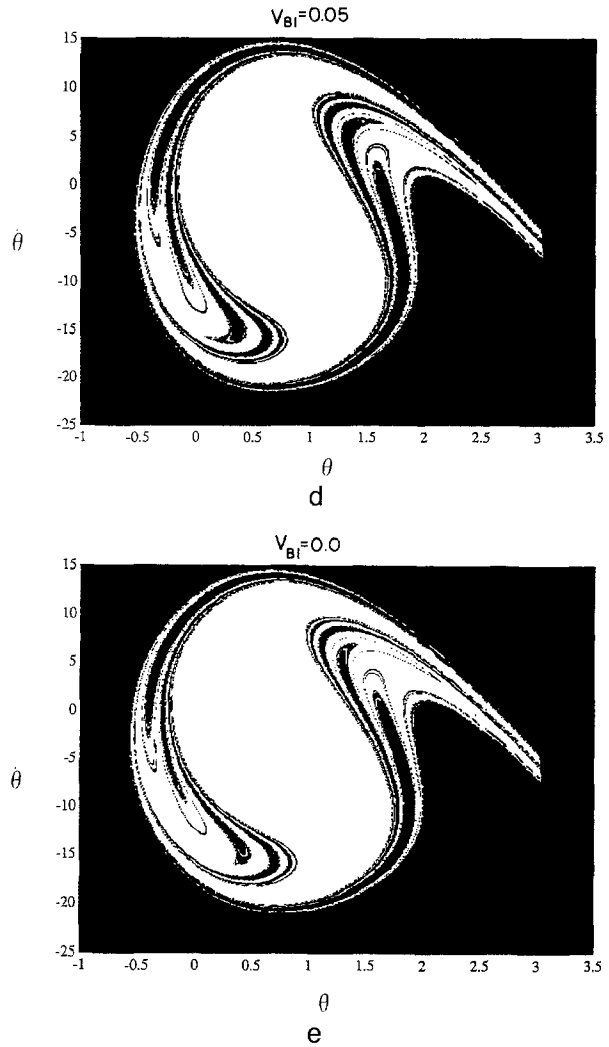

Fig. 4 (continued).

metamorphoses that the system undergoes as V_{B1} is varied for $\Omega = 19.375$ rad/sec and $\theta_{B1} = 0.2$ rad. We note that, at $\Omega = 19.375$, all the values of V_{B1} considered correspond to bounded motions in Figure 3, whereas Figure 4 shows that unbounded motions could exist at these values. The reason for this is that Figure 3 corresponds to local bifurcations, whereas Figure 4 corresponds to global bifurcations. Thus, it is clear that the response of a system to a small disturbance may be bounded, but its response to a large disturbance may be unbounded, owing to the entanglement of the stable and unstable manifolds of the saddle points. At $V_{B1} = 0.2$ (Figure 4a) the basin of attraction of bounded motions seems fractal in nature. Fingers of unbounded regions penetrate the basin of bounded motions. The fractal nature of this basin indicates sensitivity to initial conditions present at this voltage. As V_{B1} is decreased the fingers begin to subside; however, even for $V_{B1} = 0.0$ (Figure 4e) the basin of attraction of bounded motions is still corrupted by regions of unbounded motions, this is due to the effect of θ_{B1}.

Figure 5 shows the metamorphoses that the basins of attraction undergo as θ_{B1} is varied with

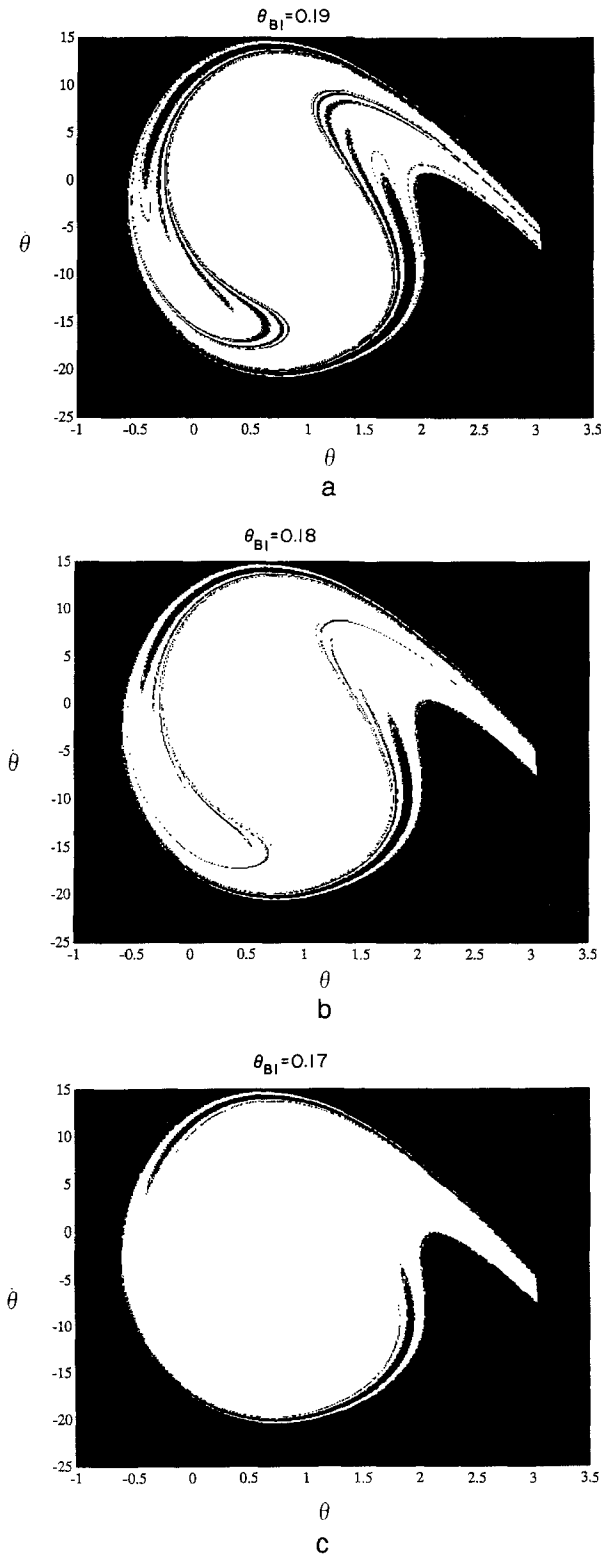

Fig. 5. Basins of attraction (θ vs. θ) for $\Omega = 19.375$ rad/sec and $V_{B1} = 0$

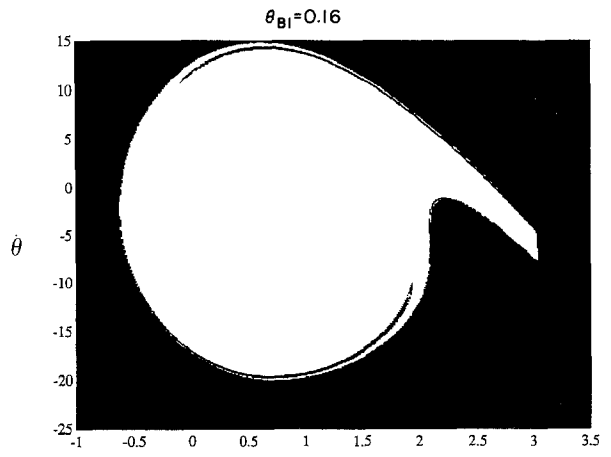

d

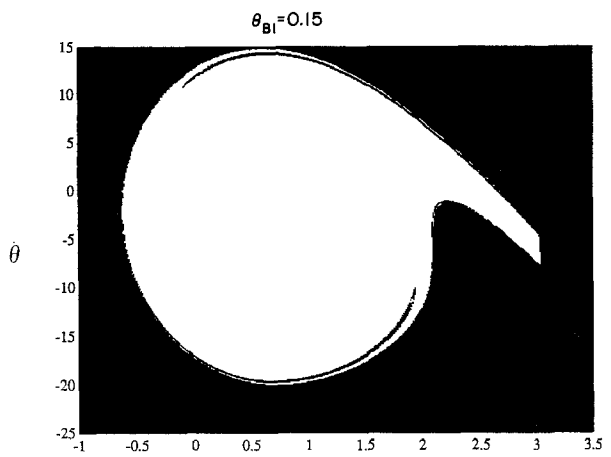

e

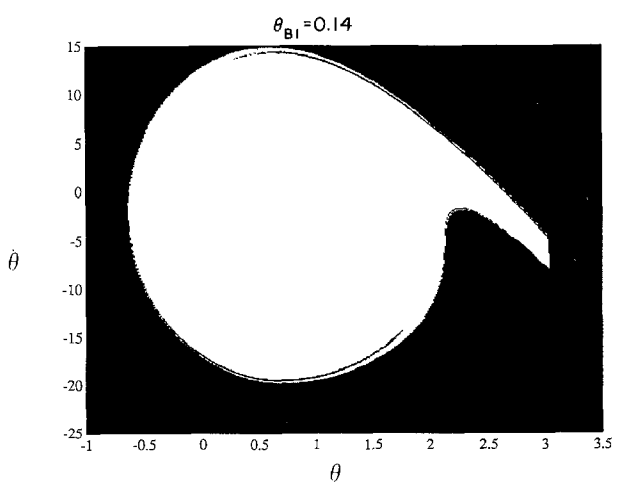

f

Fig. 5 (continued).

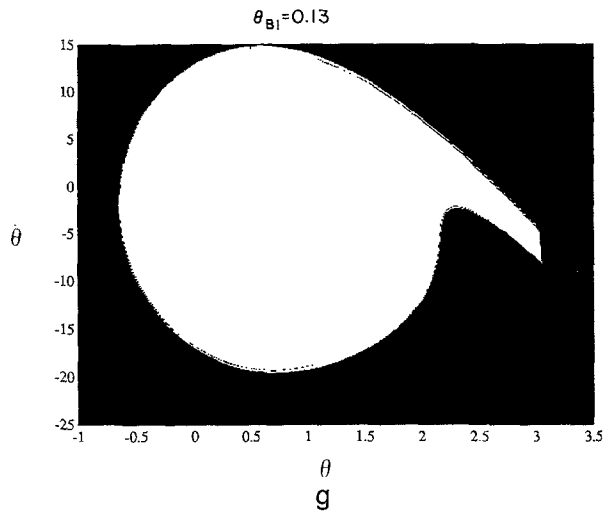

Fig. 5 (continued).

$V_{B1} = 0.0$. As θ_{B1} is decreased, the fingers of unbounded motions decrease and eventually disappear at $\theta_{B1} = 0.13$ (Figure 5g). Values of $\theta_{B1} < 0.13$ correspond to smooth basin boundaries. Eventually, at $\theta_{B1} = 0.0$ the system will have basin boundaries defined by the separatrices of the free damped oscillations of the system.

4. Perturbation Analysis

To predict the onset of the period-doubling bifurcations, which are precursors to chaos and loss of synchronism, and the saddle-node bifurcations, which are precursors to loss of synchronism, we use the method of multiple scales [3, 4] to determine a second-order approximate expression for the period-two solutions for the case $\Omega \approx 2\omega_0$. The perturbation solution is expected to be valid in a small region around the operating point θ_0. We demonstrate how a second-order analytical approximate solution can be used to predict the onset of precursors to complex dynamics and instability.

Hamdan and Nayfeh [2] used a first-order expansion, where the nonlinearities and damping terms were ordered to counter the effect of resonances due to the quasi-infinite busbar. Thus, the nonlinear, damping, and excitation terms were ordered so that their effects occur at the same order. Their solution becomes less accurate as the excitation amplitude increases because of its inability to account for the linear frequency shift caused by the excitation. In this paper, we extend their analysis to second order, thereby accounting for the linear frequency shift due to the excitation. To accomplish this, we introduce a small dimensionless parameter ε that is used as a bookkeeping device, which will be set equal to unity in the final analysis. If $\eta = 0(\varepsilon)$, then we let $\omega_R D/2H = 0(\varepsilon)$, $F_1 = 0(\varepsilon)$, $G = 0(\varepsilon)$, and we assume that $V_{B1} = 0(\varepsilon)$ and $\theta_{B1} = 0(\varepsilon)$. Quantitatively, this implies that

$$F_1 = \varepsilon f_1\,, \quad F_2 = \varepsilon f_2\,, \quad F_3 = \varepsilon f_3\,, \quad \text{and } G = \varepsilon g\,.$$

With these orderings equation (7) can be rewritten as

$$\ddot{\eta} + 2\varepsilon\mu\dot{\eta} + \omega_0^2\eta = \alpha_2\eta^2 + \alpha_3\eta^3 + \varepsilon f_1\eta\cos(\Omega t + \phi_v) + \varepsilon f_2\eta^2\cos(\Omega t + \phi_v) + \varepsilon f_3\eta^3\cos(\Omega t + \phi_v) + \varepsilon g\cos(\Omega t + \phi_e)\,, \tag{12}$$

where $\mu = \omega_R D/4H$.

We seek a uniform solution of equation (12) in the form

$$\eta(t;\varepsilon) = \varepsilon\eta_1(T_0, T_1, T_2) + \varepsilon^2\eta_2(T_0, T_1, T_2) + \varepsilon^3\eta_3(T_0, T_1, T_2) + \ldots\,, \tag{13}$$

where $T_0 = t$ is a fast scale, characterizing motions occurring at the frequencies Ω and ω_0, and $T_1 = \varepsilon t$ and $T_2 = \varepsilon^2 t$ are slow scales, characterizing the modulation of the amplitude and phase with damping, nonlinearities, and resonances due to the quasi-infinite busbar. In terms of these time scales, the time derivatives become

$$\frac{\mathrm{d}}{\mathrm{d}t} = D_0 + \varepsilon D_1 + \varepsilon^2 D_2 + \ldots \tag{14}$$

$$\frac{\mathrm{d}^2}{\mathrm{d}t^2} = D_0^2 + 2\varepsilon D_0 D_1 + \varepsilon^2(2D_0D_2 + D_1^2) + \ldots \tag{15}$$

where $D_n = \partial/\partial T_n$. To express the nearness of Ω to $2\omega_0$, we introduce the detuning parameter σ defined according to

$$\omega_0^2 = \frac{1}{4}\Omega^2 + \varepsilon\sigma\,. \tag{16}$$

This detuning is different from that used by Hamdan and Nayfeh [2]. It has the advantage of allowing larger deviations of Ω from $2\omega_0$. Substituting equations (13)–(16) into equation (12) and equating coefficients of like powers of ε, we obtain

$$D_0^2\eta_1 + \frac{1}{4}\Omega^2\eta_1 = g\cos(\Omega t + \phi_e) \tag{17}$$

$$D_0^2\eta_2 + \frac{1}{4}\Omega^2\eta_2 = -2\mu D_0\eta_1 - 2D_0D_1\eta_1 - \sigma\eta_1 + \alpha_2\eta_1^2 + f_1\eta_1\cos(\Omega T_0 + \phi_v) \tag{18}$$

$$D_0^2\eta_3 + \frac{1}{4}\Omega^2\eta_3 = -\sigma\eta_2 - 2D_0D_1\eta_2 - (D_1^2 + 2D_0D_2)\eta_1 - 2\mu(D_1\eta_1 + D_0\eta_2) + 2\alpha_2\eta_1\eta_2 + \alpha_3\eta_1^2 + f_1\eta_2\cos(\Omega T_0 + \phi_v) + f_2\eta_1^2\cos(\Omega T_0 + \phi_v)\,. \tag{19}$$

The solution of equation (17) can be expressed in either the form

$$\eta_1 = a(T_1, T_2)\cos\left[\frac{1}{2}\Omega T_0 + \beta(T_1, T_2)\right] - 2|\Lambda|\cos(\Omega T_0 + \phi_e)\,, \tag{20}$$

or the form

$$\eta_1 = A(T_1, T_2)e^{1/2(i\Omega T_0)} + \overline{A}(T_1, T_2)e^{-1/2(i\Omega T_0} + \Lambda e^{i\Omega T_0} + \overline{\Lambda}e^{-i\Omega T_0}\,, \tag{21}$$

where $\overline{A}$ is the complex conjugate of A and

$$\Lambda = -\frac{2g}{3\Omega^2} e^{i\phi_e} . \tag{22}$$

Comparing equations (20) and (21) shows that

$$A = \frac{1}{2} ae^{i\beta} . \tag{23}$$

Substituting equation (21) into equation (18) leads to

$$\begin{aligned} D_0^2\eta_2 + \frac{1}{4}\Omega^2\eta_2 = &\left[-i\Omega(D_1A + \mu A) - \sigma A + 2\alpha_2\Lambda\overline{A}\right. \\ &\left. + \frac{1}{2} f_1\overline{A}e^{i\phi_v}\right]e^{1/2(i\Omega T_0)} + [-2i\mu\Omega\Lambda - \sigma\Lambda + \alpha_2A^2]e^{i\Omega T_0} \\ &+ \left[2\alpha_2A\Lambda + \frac{1}{2} f_1Ae^{i\phi_v}\right]e^{3/2(i\Omega T_0} + \left[\alpha_2(A\overline{A} + \Lambda\overline{\Lambda}) + \frac{1}{2} f_1\overline{\Lambda}e^{i\phi_v}\right] \\ &+ \left[\alpha_2\Lambda^2 + \frac{1}{2} f_1\Lambda e^{i\phi_v}\right]e^{2i\Omega T_0} + cc , \end{aligned} \tag{24}$$

where *cc* stands for the complex conjugate of the preceding terms. Eliminating the secular terms (terms that render the expansion nonuniform for large t) in equation (24), we have

$$-i\Omega D_1A - i\Omega\mu A - \sigma A + \overline{A}\Gamma e^{i\phi_{ee}} = 0 , \tag{25}$$

where

$$\Gamma e^{i\phi_{ee}} = 2\alpha_2\Lambda + \frac{1}{2} f_1e^{i\phi_v} . \tag{26}$$

Hence, the solution of equation (24) can be written as

$$\begin{aligned} \eta_2 = &-\frac{4}{3\Omega^2}[\alpha_2A^2 - (2i\mu\Omega + \sigma)\Lambda]e^{i\Omega T_0} - \frac{A}{2\Omega^2}\Gamma e^{i((3/2)\Omega T_0 + \phi_{ee})} \\ &+ \frac{4}{\Omega^2}\left[\alpha_2(A\overline{A} + \Lambda\overline{\Lambda}) + \frac{1}{2} f_1\overline{\Lambda}e^{i\phi_v}\right] \\ &- \frac{4}{15\Omega^2}\left[\alpha_2\Lambda^2 + \frac{1}{2} f_1\Lambda e^{i\phi_v}\right]e^{2i\Omega T_0} + cc . \end{aligned} \tag{27}$$

Substituting equations (21) and (27) into equation (19) yields

$$\begin{aligned} D_0^2\eta_3 + \frac{1}{4}\Omega^2\eta_3 = &-i\Omega D_2A - D_1^2A - 2\mu D_1A \\ &- \frac{8\alpha_2}{3\Omega^2}[-(2i\mu\Omega + \sigma)\Lambda\overline{A} + \alpha_2A^2\overline{A}] - \frac{\alpha_2A\overline{\Lambda}}{\Omega^2}\Gamma e^{i\phi_{ee}} \\ &+ \frac{8\alpha_2}{\Omega^2}\left[2\alpha_2A^2\overline{A} + 2\alpha_2A\Lambda\overline{\Lambda} + \frac{1}{2} f_1A(\overline{\Lambda}e^{i\phi_v} + \Lambda e^{-i\phi_v})\right] \\ &+ 6\alpha_3A\Lambda\overline{\Lambda} + 3\alpha_3A^2\overline{A} - \frac{Af_1\Gamma}{4\Omega^2} e^{i(\phi_{ee} - \phi_v)} + f_2A(\overline{\Lambda}e^{i\phi_v} + \Lambda e^{-i\phi_v}) + NST + cc . \end{aligned} \tag{28}$$

It follows from equation (25) that

$$D_1\bar{A} = -\left(\mu + \frac{i\sigma}{\Omega}\right)\bar{A} + \frac{i}{\Omega} A\Gamma e^{-i\phi_{ee}} \tag{29}$$

and

$$D_1^2 A = \left[\mu^2 - \frac{2i\mu\sigma}{\Omega} + \frac{\Gamma^2 - \sigma^2}{\Gamma^2}\right]A + \frac{2i\mu}{\Omega}\bar{A}\Gamma e^{i\phi_{ee}} . \tag{30}$$

Eliminating the secular terms from equation (28) and using equations (25) and (30), we obtain

$$\begin{aligned} &-i\Omega D_2 A + \left[\mu^2 - \frac{\Gamma^2 - \sigma^2}{\Omega^2} - \frac{\alpha_2\bar{\Lambda}\Gamma}{\Omega^2} e^{i\phi_{ee}} + \left(6\alpha_3 + \frac{16\alpha_2^2}{\Omega^2}\right)\Lambda\bar{\Lambda}\right. \\ &\quad \left. + (\bar{\Lambda}e^{i\phi_v} + \Lambda e^{-i\phi_v})\left(\frac{4\alpha_2 f_1}{\Omega^2} + f_2\right) - \frac{\Gamma f_1}{4\Gamma^2} e^{i(\phi_{ee} - \phi_v)}\right]A \\ &\quad + \left(3\alpha_3 + \frac{40\alpha_2^2}{3\Omega^2}\right)A^2\bar{A} + \frac{8\alpha_2}{3\Omega^2}(2i\mu\Omega + \sigma)\Lambda\bar{A} = 0 . \end{aligned} \tag{31}$$

Using the method of reconstitution [9], we form the derivative of A with respect to t by substituting equations (25) and (31) into equation (14), putting $\varepsilon = 1$, and obtaining

$$i\Omega(\dot{A} + \mu_e A) + \sigma_e A - 4\alpha_e A^2\bar{A} - \bar{A}\hat{\Gamma}e^{i\hat{\phi}_e} = 0 , \tag{32}$$

where the overdot indicates the derivative with respect to t,

$$\mu_e = \mu - \frac{2\alpha_2 g\Gamma}{3\Omega^5}\sin(\phi_{ee} - \phi_e) + \frac{\Gamma f_1}{4\Omega^3}\sin(\phi_{ee} - \phi_v) , \tag{33}$$

$$\begin{aligned} \sigma_e = \sigma - \mu^2 &+ \frac{\Gamma^2 - \sigma^2}{\Omega^2} - \left(\frac{2g}{3\Omega^2}\right)^2\left(6\alpha_3 + \frac{16\alpha_2^2}{\Omega^2}\right) \\ &+ \frac{4g}{3\Omega^2}\left(f_2 + \frac{4\alpha_2 f_1}{\Omega^2}\right)\cos(\phi_v - \phi_e) \\ &- \frac{2\alpha_2 g\Gamma}{3\Omega^4}\cos(\phi_{ee} - \phi_e) + \frac{\Gamma f_1}{4\Omega^2}\cos(\phi_{ee} - \phi_v) , \end{aligned}$$

$$\alpha_e = \frac{10\alpha_2^2}{3\Omega^2} + \frac{3}{4}\alpha_3 , \tag{35}$$

and

$$\hat{\Gamma}e^{i\hat{\phi}_e} = \Gamma e^{i\phi_{ee}} - \frac{16\alpha_2 g}{9\Omega^4}(2i\mu\Omega + \sigma)e^{i\phi_e} . \tag{36}$$

Expressing A in the polar form (23) and separating real and imaginary parts in equation (32), we obtain

$$\Omega(\dot{a} + \mu_e a) - a\hat{\Gamma}\sin\gamma = 0 \tag{37}$$

$$-\Omega a\dot{\beta} + \sigma_e a - \alpha_e a^3 - a\hat{\Gamma}\cos\gamma = 0 , \tag{38}$$

where

$$\gamma = \hat{\phi}_e - 2\beta \,, \tag{39}$$

Therefore, to the second approximation

$$\begin{aligned}\eta = {} & a\cos\left[\frac{1}{2}(\Omega t + \hat{\phi}_e - \gamma)\right] - \frac{4g}{3\Omega^2}\cos(\Omega t + \phi_e) \\ & + \frac{32\mu g}{9\Omega^3}\sin(\Omega t + \phi_e) - \frac{16\sigma g}{9\Omega^4}\cos(\Omega t + \phi_e) \\ & - \frac{2a^2\alpha_2}{3\Omega^2}\cos(\Omega t + \hat{\phi}_e - \gamma) - \frac{32\alpha_2 g^2}{135\Omega^6}\cos[2(\Omega t + \phi_e)] \\ & - \frac{af_1}{4\Omega^2}\cos\left[\frac{3}{2}\Omega t + \phi_v + \frac{1}{2}(\hat{\phi}_e - \gamma)\right] + \frac{2\alpha_2}{\Omega^2}\left(a^2 + \frac{16g^2}{9\Omega^4}\right) \\ & - \frac{8f_1 g}{3\Omega^4}\cos(\phi_v - \phi_e) + \frac{2\alpha_2 ag}{3\Omega^4}\cos\left[\frac{3}{2}\Omega t + \phi_e + \frac{1}{2}(\hat{\phi}_e - \gamma)\right] \\ & + \frac{8f_1 g}{45\Omega^4}\cos(2\Omega t + \phi_e + \phi_v)\,. \end{aligned} \tag{40}$$

Consequently,

$$\begin{aligned}\Delta\theta = {} & \theta_{B1}\cos(\Omega t + \phi_\theta) + a\cos\left[\frac{1}{2}(\Omega t + \hat{\phi}_e - \gamma)\right] - \frac{4g}{3\Omega^2}\cos(\Omega t + \phi_e) \\ & + \frac{32\mu g}{9\Omega^3}\sin(\Omega t + \phi_e) - \frac{16\sigma g}{9\Omega^4}\cos(\Omega t + \phi_e) - \frac{2a^2\alpha_2}{3\Omega^2}\cos(\Omega t + \hat{\phi}_e - \gamma) \\ & + \frac{2\alpha_2 ag}{3\Omega^4}\cos\left[\frac{3}{2}\Omega t + \phi_e + \frac{1}{2}(\hat{\phi}_e - \gamma)\right] \\ & - \frac{af_1}{4\Omega^2}\cos\left[\frac{3}{2}\Omega t + \phi_v + \frac{1}{2}(\hat{\phi}_e - \gamma)\right] + \frac{2\alpha_2}{\Omega^2}\left(a^2 + \frac{16g^2}{9\Omega^4}\right) \\ & - \frac{8f_1 g}{3\Omega^4}\cos(\phi_v - \phi_e) - \frac{32\alpha_2 g^2}{135\,\Omega^6}\cos[2(\Omega t + \phi_e)] \\ & + \frac{8f_1 g}{45\Omega^4}\cos(2\Omega t + \phi_e + \phi_v) + \ldots\,. \end{aligned} \tag{41}$$

The periodic solutions of equation (12) correspond to the fixed points of equations (37)–(39); that is, $\dot{a} = \dot{\beta} = 0$. Hence equations (37)–(39) become

$$\Omega\mu_e a - \hat{\Gamma} a \sin\gamma = 0\,, \tag{42}$$

$$\sigma_e a - \alpha_e a^3 - \hat{\Gamma} a\cos\gamma = 0\,. \tag{43}$$

It follows from equations (42) and (43) that the fixed points can be either trivial (i.e., $a = 0$) or nontrivial (i.e., $a \neq 0$). When $a = 0$ it follows from equations (5) and (41) that the variations in the

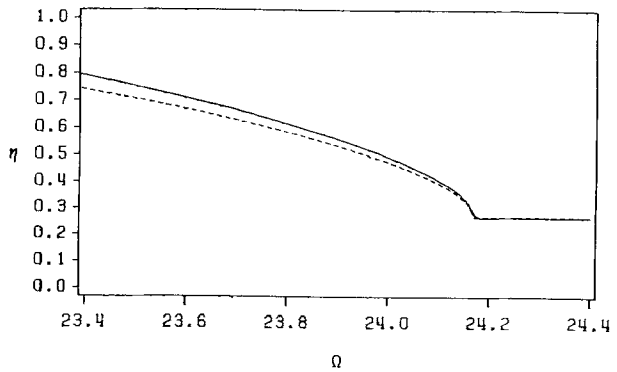

Fig. 6. Frequency-response curve when $V_{B1} = \theta_{B1} = 0.2$: numerical simulation (– – –); perturbation results (____).

rotor angle of the machine are given by

$$\Delta\theta = \theta_{B1}\cos(\Omega t + \phi_\theta) - \frac{4g}{3\Omega^2}\cos(\Omega t + \phi_e) + \frac{32\mu g}{9\Omega^3}\sin(\Omega t + \phi_e)$$
$$- \frac{16\sigma g}{9\Omega^4}\cos(\Omega t + \phi_e) + \frac{32\alpha_2 g^2}{9\Omega^6} - \frac{8f_1 g}{3\Omega^4}\cos(\phi_v - \phi_e)$$
$$- \frac{32\alpha_2 g^2}{135\,\Omega^6}\cos[2(\Omega t + \phi_e)] + \frac{8f_1 g}{45\Omega^4}\cos(2\Omega t + \phi_e + \phi_v) + \ldots . \tag{44}$$

When $a \neq 0$, one can eliminate γ from equations (42) and (43) to obtain the frequency-response equation

$$a^2 = \frac{1}{\alpha_e}\left[\sigma_e \pm \sqrt{\hat{\Gamma} - \Omega^2\mu_e^2}\right], \tag{45}$$

which relates the amplitude of the response to the frequency and amplitude of the excitation. The, γ, can be calculated from either equation (42) or equation (43). Substituting these values into equation (40), one can calculate the maximum value of η. A typical variation of this maximum with the excitation frequency is shown in Figure 6.

5. Comparison of Perturbation Solution with Numerical Simulations

To analyze the accuracy of the closed-form analytical solution, we compare it with numerical simulations of equations (1)–(3). For a given Ω, we calculate a from equation (45) and then calculate γ from equations (42) and (43). Substituting the values of a and γ into equations (40), we determine η and $\dot{\eta}$. A typical long-time history of the response and its phase portrait are shown in Figures 7a and 7b for $\Omega = 26$ rad/sec. Figures 7a and 7b show that there is good agreement between the results of the numerical simulation and the perturbation solution. To form an overall comparison, we plot in Figure 6 the maximum values of η obtained from the perturbation solution (frequency-response curve) and the numerical simulation. Again we have good agreement.

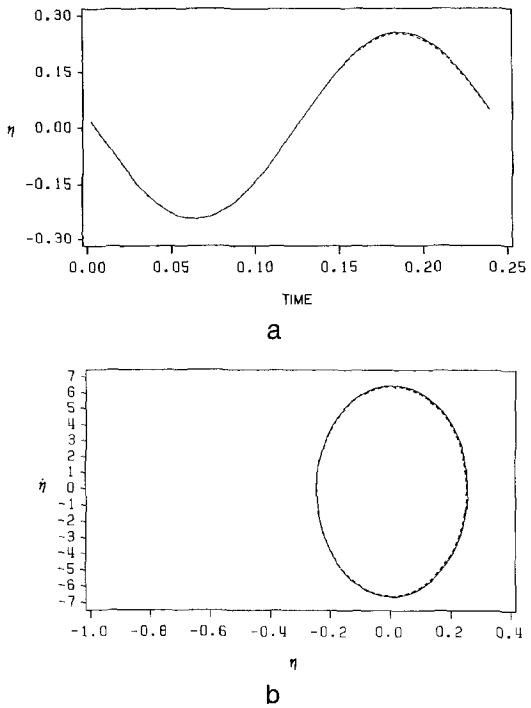

Fig. 7. Comparison of the results of the perturbation solution with those obtained by numerical simulation: (a) time-history and (b) phase-plane comparison of perturbation (- - -) and numerical (____) solutions for $\Omega = 26.0$ rad/sec.

6. Stability of Period-One and Period-Two Solutions

To determine the stability of the periodic solutions predicted by the perturbation analysis, we use Floquet theory [10]. We introduce a small disturbance $\xi(t)$ to obtain

$$\hat{\eta}(t) = \eta(t) + \xi(t) . \tag{46}$$

Thus, a given periodic solution $\eta(t)$ is stable if $\xi(t)$ decays with time and it is unstable if $\xi(t)$ grows with time. Substituting equation (46) into equation (7) and linearizing the result, we obtain the variational equation

$$\frac{d^2\xi}{dt^2} + \frac{\omega_R D}{2H}\frac{d\xi}{dt} + [K - 2\alpha_2\eta - 3\alpha_3\eta^2 - F_1\cos(\Omega t + \phi_v)]\xi = 0 , \tag{47}$$

which is a linear-differential equation with periodic coefficients having the period $T = 4\pi/\Omega$ when $\eta(t)$ is given by equation (40) and $a \neq 0$ and the period $T = 2\pi/\Omega$ when $\eta(t)$ is given by equation (40) and $a = 0$. Using Floquet theory, we calculate two linearly independent solutions of equation (47) by using the initial conditions (a) $\xi_1(0) = 1$ and $\dot{\xi}_1(0) = 0$ and (b) $\xi_2(0) = 0$ and $\dot{\xi}_2(0) = 1$. Then, we form the Monodromy matrix

$$\begin{bmatrix} \xi_1(T) & \dot{\xi}_1(T) \\ \xi_2(T) & \dot{\xi}_2(T) \end{bmatrix}$$

whose eigenvalues yield the Floquet multipliers λ_1 and λ_2. The long-time behavior of $\xi(t)$ and hence the stability of the periodic solution $\eta(t)$ depends on the magnitudes of the Floquet multipliers. If both of them lie inside the unit circle in the complex plane, $\xi(t)$ decays to zero with time and $\eta(t)$ is stable. If one of these multipliers lies outside the unit circle, $\xi(t)$ grows with time and hence $\xi(t)$ is unstable. Starting with system parameters corresponding to a stable solution and varying one of these parameters, such as Ω or V_{B1} or θ_{B1}, one finds that, for the single-degree-of-freedom system being studied, λ can leave the unit circle along the real axis through either $+1$ or -1. If λ leaves the unit circle through $+1$, then at bifurcation, equation (47) possesses a periodic solution of period T, indicating that the new solution has the period T. Because $\eta(t)$ is asymmetric, the bifurcation will lead to a jump; that is, the bifurcation is a cyclic-fold or saddle-node bifurcation and the instability is called a tangent instability. If λ leaves the unit circle through -1, then at bifurcation, equation (47) possesses a periodic solution having the period 2T, indicating that the resulting solution is periodic having the period 2T; signalling a period-doubling bifurcation.

Applying Floquet theory to the analytically predicted periodic solution (40), we calculated the bifurcation curves along which the periodic solution loses stability. The results are compared with the numerically calculated curves in Figure 8. The analytical solution (Δ, $\times$) predicts the loss of stability of the period-one solution through a saddle-node bifurcation very accurately, as can be seen in Figure 8 (curves P_3 and P_4). Moreover, the analytical solution ($+$) predicts fairly well the occurrence of period-doubling bifurcations leading to chaos, as can be seen in Figure 8 (curve P_2).

7. Conclusions

We have demonstrated by numerical simulation the existence of complex dynamics in a single-machine quasi-infinite busbar system due to the simultaneous occurrence of a principal parametric resonance and a subharmonic resonance of order one-half. By decreasing the frequency of excitation we have shown that oscillatory solutions (limit cycles) lose their stability through a series of period-doubling bifurcations, leading to chaos and unbounded motions (loss of synchronism). We formulated a second-order approximate solution that improves on the accuracy of the

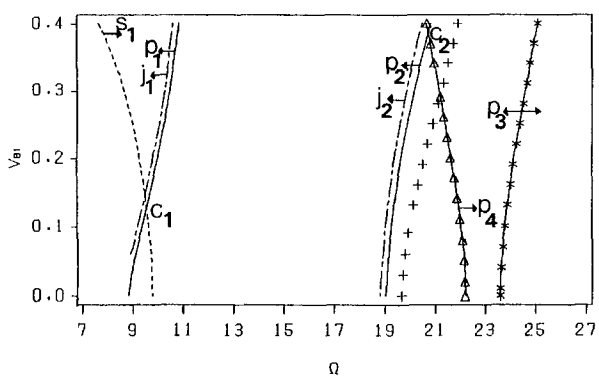

Fig. 8. Comparison of saddle-node and period-doubling bifurcations predicted by the perturbation solution with those obtained by numerical simulation.

solution given by Hamdan and Nayfeh [2]. Our solution accounts for the linear frequency shift caused by the excitation. The loss of stability of the second-order solution, which is a precursor to chaos and unbounded motions, agrees fairly well with the numerical simulations.

Acknowledgement

This work was supported by the National Science Foundation under Grant No. MSM-8521748.

Appendix A

The parameters of the machine have been taken from Table D3 of Appendix D of the textbook of Anderson and Fouad [8]. They are

$$\text{Rated MVA} = 160,\ \text{Rated PF} = 0.85,\ \text{Rated KV} = 15,$$
$$\omega_R = 120\pi \text{ rad./sec.},\quad X'_d = 0.245,\quad \text{H} = 2.37\ \text{S},\quad P_m = 1 \text{ per unit.}$$

The rest of the parameters of the SMQIBS are

$$X_{line} = 0.4 \text{ per unit},\quad V_{B0} = 1 \text{ per unit},\quad V_{B1} = 0.2 \text{ per unit},$$
$$\theta_{B0} = 0,\quad \theta_{B1} = 0.2 \text{ rad},\quad \text{D} = 0.008 \text{ units}$$
$$X_G = X_{line} + X'_d = 0.645 \text{ per unit}.$$

References

1. Tamura, Y., Yorino, N., Mori, H., and Iwamoto, S., 'On the possibility of parametric resonance in power systems – a new concept of power system stability', *Proceedings PSCC*, 1984, 1894–1898.
2. Hamdan, A. M. A. and Nayfeh, A. H., 'The effect of nonlinearities on the response of a single-machine-quasi-infinite-busbar system', *IEEE Transactions on Power Systems* PWRS-4, 1989, 843–849.
3. Nayfeh, A. H., *Introduction to Perturbation Techniques*, Wiley-Interscience, New York, 1981.
4. Nayfeh, A. H., *Perturbation Methods*, Wiley-Interscience, New York, 1973.
5. Grebogi, C., Ott, E., and Yorke, J., 'Metamorphoses of basin boundaries in non-linear dynamics systems', *Physical Review Letters* **56**, 1986, 1011–1014.
6. Nayfeh, A. H. and Sanchez, N. E., 'Bifurcations in a forced softening Duffing oscillator', *International Journal of Non-Linear Mechanics* **24**, 1989, 483–497.
7. Soliman, F. M. and Thompson, J. M. T., 'Integrity measures quantifying the erosion of smooth and fractal basins of attraction', *Journal of Sound and Vibration* **135**, 1989, 453–474.
8. Anderson, P. M. and Fouad, A. A., *Power System Control and Stability*, Iowa State University Press, Ames, IA, 1977.
9. Nayfeh, A. H., 'Perturbation methods in nonlinear dynamics', *Nonlinear Dynamics Aspects of Particle Accelerators*, Lecture Notes in Physics No. 247, Springer-Verlag, New York, 1986, 238–314.
10. Nayfeh, A. H. and Mook, D. T., *Nonlinear Oscillations*, Wiley-Interscience, New York, 1979.